Vehicle System Dynamics: International Journal of Vehicle Mechanics and Mobility

Publication details, including instructions for authors and subscription information:
http://www.tandfonline.com/loi/nvsd20

Semi-active H∞ control of high-speed railway vehicle suspension with magnetorheological dampers

Lu-Hang Zong [a], Xing-Long Gong [a], Shou-Hu Xuan [a] & Chao-Yang Guo [a]

[a] CAS Key Laboratory of Mechanical Behavior and Design of Materials, Department of Modern Mechanics, University of Science and Technology of China (USTC), Hefei, 230027, People's Republic of China

Version of record first published: 24 Jan 2013.

To cite this article: Lu-Hang Zong , Xing-Long Gong , Shou-Hu Xuan & Chao-Yang Guo (2013): Semi-active H∞ control of high-speed railway vehicle suspension with magnetorheological dampers, Vehicle System Dynamics: International Journal of Vehicle Mechanics and Mobility, DOI:10.1080/00423114.2012.758858

To link to this article: http://dx.doi.org/10.1080/00423114.2012.758858

Vehicle System Dynamics, 2013
http://dx.doi.org/10.1080/00423114.2012.758858

Taylor & Francis
Taylor & Francis Group

Semi-active H∞ control of high-speed railway vehicle suspension with magnetorheological dampers

Lu-Hang Zong, Xing-Long Gong*, Shou-Hu Xuan and Chao-Yang Guo

CAS Key Laboratory of Mechanical Behavior and Design of Materials, Department of Modern Mechanics, University of Science and Technology of China (USTC), Hefei 230027, People's Republic of China

(*Received 25 August 2012; final version received 10 December 2012*)

In this paper, semi-active H∞ control with magnetorheological (MR) dampers for railway vehicle suspension systems to improve the lateral ride quality is investigated. The proposed semi-active controller is composed of a H∞ controller as the system controller and an adaptive neuro-fuzzy inference system (ANFIS) inverse MR damper model as the damper controller. First, a 17-degree-of-freedom model for a full-scale railway vehicle is developed and the random track irregularities are modelled. Then a modified Bouc–Wen model is built to characterise the forward dynamic characteristics of the MR damper and an inverse MR damper model is built with the ANFIS technique. Furthermore, a H∞ controller composed of a yaw motion controller and a rolling pendulum motion (lateral motion + roll motion) controller is established. By integrating the H∞ controller with the ANFIS inverse model, a semi-active H∞ controller for the railway vehicle is finally proposed. Simulation results indicate that the proposed semi-active suspension system possesses better attenuation ability for the vibrations of the car body than the passive suspension system.

Keywords: railway vehicles; semi-active suspension; H∞ control; magnetorheological fluid damper; ANFIS inverse model

1. Introduction

Nowadays, many countries have been devoted to develop the high-speed railway vehicle technology because it has been proved to be an efficient and economical transportation method. However, the increase in the train's speed will amplify the train's vibrations significantly, which will induce an obvious decrease in the ride stability and ride quality. Thus, it is crucial to suppress the vibrations of railway vehicles to improve the ride comfort and safety. There are three types of suspension systems, including passive, semi-active, and active suspension. Among them, the magnetorheological (MR) damper-based semi-active suspension has attracted increasing attentions, due to its better performance than passive suspension and its low power requirements and inexpensive hardware in comparison with active suspension. The MR damper-based semi-active controller usually works via a two-step progress [1]. First, a system controller determines the desired control force according to the responses; then a damper controller adjusts the command current applied to the MR damper to track the desired control force. Thus, the successful application of the MR damper-based semi-active controller

*Corresponding author. Email: gongxl@ustc.edu.cn

is determined practically by two aspects: one is the selection of an appropriate control strategy and the other is the establishment of the accurate damper controller.

The performance of a semi-active control system is highly dependent on the control strategy, which is the core of the system controller. Various control strategies, such as skyhook, groundhook and hybrid control [2], linear optimal control [3], gain scheduling control [4], adaptive control [5], H∞ control [6,7], preview control [8], sliding mode control [9], fuzzy logic control [10], neural network control [11], and human-simulated intelligent control [12] have been proposed to improve the performance of automobile vehicles and structures. However, researches dealing with active or semi-active control of rail vehicle suspension are relatively few. O'Neill and Wale [13] first adopted skyhook control to suppress the lateral vibrations of railway vehicles. Atray and Roschke [14] proposed a neuro-fuzzy controller for a two-degree-of-freedom (DOF) quarter car model of the railway vehicle. Yang *et al*. [15] built an adaptive fuzzy controller based on the acceleration feedback. Orukpe *et al*. [16] investigated model predictive control technology based on the mixed H2/H∞ control approach for active suspension control to suppress the vertical vibrations of a railway vehicle. Liao and Wang [1] designed a semi-active linear quadratic Gaussian (LQG) controller using the acceleration feedback for a nine DOF railway vehicle. Later, they enlarged the controller to a 17-DOF model [17,18]. With faster speed and lighter bodies introduced to the high-speed train, the controller should be designed to be more robust, i.e. to operate effectively through a full range of operational conditions. H∞ control has been proved to be an effective way in the automobile vehicle suspensions [6,7] and railway vertical suspension [16]. Here, it is adopted to attenuate the lateral vibration of the high-speed train.

Another important part of a semi-active controller is the damper controller, which is used to determine the input current to track the desired force. The damping force generated by the MR damper is decided by the input current, the piston relative velocity, and displacement of the MR damper, among which only the input current can be directly controlled. Thus, it is important to build an accurate damper controller to generate the appropriate input current. For data, some force feedback methods were proposed to build the damper controller [19–21]. Although these methods are simple, the extra force sensors will increase the cost of the system. In this sense, some inverse-model-based methods have been proposed to build the damper controller.

Inverse MR damper models are always derived from forward models, so it is necessary to establish the forward models first. During the past decades, both nonparametric and parametric models have been developed to describe the forward behaviours of MR dampers. The parametric models include the Bingham model [22], nonlinear hysteretic biviscous model [23], viscoelastic–plastic model [24], phenomenological model [25], LuGre model [26], Dahl model [27], and hyperbolic tangent function-based model [28]. The nonparametric models include polynomial model [29], neural network model [30], and neuro-fuzzy model [31]. Among them, the phenomenological model is one of the most accurate models in describing the forward behaviour of MR dampers. However, the corresponding inverse model is difficult to obtain due to its nonlinearity and complexity. For some other forward models, including the polynomial model [29], sigmoid function-based model [32], modified LuGre model [33], and simplified phenomenological model [34], their inverse dynamic model can be analytically determined. Moreover, neural networks [35] and the adaptive neuro-fuzzy inference system (ANFIS) [36] are also used to develop the inverse MR damper models because of their strong nonlinearity disposing ability. Among these methods, the neural networks and ANFIS methods can accurately predict the command current of the MR dampers. For this reason, the ANFIS method is applied to build the damper controller in this paper.

This paper first combines the H∞ control strategy with the ANFIS technology and proposes a robust MR damper-based semi-active controller for high-speed railway vehicle suspensions.

This semi-active system is easy to design as only the car body motions are considered in the H∞ controller and costless in practical use as it only needs four accelerometer sensors and does not need any force sensors. First, a 17-DOF model of a full-scale railway vehicle integrated with MR dampers in its secondary suspension system is developed, and the random track irregularities are modelled. Then a modified Bouc–Wen model is built to characterise the forward dynamic characteristics of the MR damper and an inverse MR damper model is built with the ANFIS technique. Furthermore, a H∞ controller of the car body composed of a yaw motion controller and a rolling pendulum motion controller is established to generate the active force. By integrating the H∞ controller with the ANFIS inverse model, a semi-active H∞ controller is proposed finally and its performances are evaluated by simulation.

2. Analytical model of the railway vehicle

2.1. *Railway vehicle dynamics*

The high-speed train studied in the paper is composed of one car body, two bogies, and four wheelsets. The two bogies, which are identified as the front and rear bogies, are connected to the car body by the secondary suspension. Each of the two bogies is also connected to two wheelsets (identified as the leading wheelset and the trailing wheelset) by the primary suspension. Figure 1 shows the analytical model of the full-scale railway vehicle integrated with MR dampers. The motions of the car body, bogies, and wheelsets of the railway vehicle involved in the modelling are listed in Table 1. The train system contains 17-DOFs in total. The governing equations of the railway vehicle dynamics are presented as follows.

(a) *Car body dynamics*:

$$\begin{aligned} &M_c\ddot{y}_c + K_{2y}(y_c + l\varphi_c - h_1\theta_c - y_{t1} - h_3\theta_{t1}) + C_{2y}(\dot{y}_c + l\dot{\varphi}_c - h_2\dot{\theta}_c - \dot{y}_{t1} - h_5\dot{\theta}_{t1}) \\ &\quad + K_{2y}(y_c - l\varphi_c - h_1\theta_c - y_{t2} - h_3\theta_{t2}) + C_{2y}(\dot{y}_c - l\dot{\varphi}_c - h_2\dot{\theta}_c - \dot{y}_{t2} - h_5\dot{\theta}_{t2}) \\ &\quad = u_1 + u_2 \end{aligned} \tag{1}$$

$$\begin{aligned} &J_{cz}\ddot{\varphi}_c + K_{2y}l(y_c + l\varphi_c - h_1\theta_c - y_{t1} - h_3\theta_{t1}) + C_{2y}l(\dot{y}_c + l\dot{\varphi}_c - h_2\dot{\theta}_c - \dot{y}_{t1} - h_5\dot{\theta}_{t1}) \\ &\quad - K_{2y}l(y_c - l\varphi_c - h_1\theta_c - y_{t2} - h_3\theta_{t2}) - C_{2y}l(\dot{y}_c - l\dot{\varphi}_c - h_2\dot{\theta}_c - \dot{y}_{t2} - h_5\dot{\theta}_{t2}) \\ &\quad + K_{2x}b_2^2(\varphi_c - \varphi_{t1}) + C_{2x}b_3^2(\dot{\varphi}_c - \dot{\varphi}_{t1}) + K_{2x}b_2^2(\varphi_c - \varphi_{t2}) + C_{2x}b_3^2(\dot{\varphi}_c - \dot{\varphi}_{t2}) \\ &\quad = u_1 l - u_2 l \end{aligned} \tag{2}$$

$$\begin{aligned} &J_{cx}\ddot{\theta}_c - K_{2y}h_1(y_c + l\varphi_c - h_1\theta_c - y_{t1} - h_3\theta_{t1}) - C_{2y}h_2(\dot{y}_c + l\dot{\varphi}_c - h_2\dot{\theta}_c - \dot{y}_{t1} - h_5\dot{\theta}_{t1}) \\ &\quad - K_{2y}h_1(y_c - l\varphi_c - h_1\theta_c - y_{t2} - h_3\theta_{t2}) - C_{2y}h_2(\dot{y}_c - l\dot{\varphi}_c - h_2\dot{\theta}_c - \dot{y}_{t2} - h_5\dot{\theta}_{t2}) \\ &\quad + K_{2z}b_2^2(\theta_c - \theta_{t1}) + C_{2z}b_3^2(\dot{\theta}_c - \dot{\theta}_{t1}) + K_{2z}b_2^2(\theta_c - \theta_{t2}) + C_{2z}b_3^2(\dot{\theta}_c - \dot{\theta}_{t2}) \\ &\quad = -u_1 h_2 - u_2 h_2 \end{aligned} \tag{3}$$

(b) *Bogie dynamics* ($i = 1 \sim 2$):

$$\begin{aligned} &M_t\ddot{y}_{ti} - K_{2y}(y_c - (-1)^i l\varphi_c - h_1\theta_c - y_{ti} - h_3\theta_{ti}) - C_{2y}(\dot{y}_c - (-1)^i l\dot{\varphi}_c - h_2\dot{\theta}_c - \dot{y}_{ti} - h_5\dot{\theta}_{ti}) \\ &\quad + K_{1y}(y_{ti} + l_1\varphi_{ti} - h_4\theta_{ti} - y_{w(2i-1)}) + C_{1y}(\dot{y}_{ti} + l_1\dot{\varphi}_{ti} - h_4\dot{\theta}_{ti} - \dot{y}_{w(2i-1)}) \\ &\quad + K_{1y}(y_{ti} - l_1\varphi_{ti} - h_4\theta_{ti} - y_{w(2i)}) + C_{1y}(\dot{y}_{ti} - l_1\dot{\varphi}_{ti} - h_4\dot{\theta}_{ti} - \dot{y}_{w(2i)}) \\ &\quad = -u_i \end{aligned} \tag{4}$$

Figure 1. Analytical model of a full-scale railway vehicle integrated with MR dampers.

Table 1. Lateral motions of the 17-DOF railway vehicle model.

Component		Motion		
		Lateral	Yaw	Roll
Car body		y_c	φ_c	θ_c
Bogie	Front bogie frame	y_{t1}	φ_{t1}	θ_{t1}
	Rear bogie frame	y_{t2}	φ_{t2}	θ_{t2}
Wheelset	Front bogie leading wheelset	y_{w1}	φ_{w1}	–
	Front bogie trailing wheelset	y_{w2}	φ_{w2}	–
	Rear bogie leading wheelset	y_{w3}	φ_{w3}	–
	Rear bogie trailing wheelset	y_{w4}	φ_{w4}	–

$$
\begin{aligned}
&J_{tz}\ddot{\varphi}_{ti} - K_{2x}b_2^2(\varphi_c - \varphi_{ti}) - C_{2x}b_3^2(\dot{\varphi}_c - \dot{\varphi}_{ti}) + K_{1y}l_1(y_{ti} + l_1\varphi_{ti} - h_4\theta_{ti} - y_{w(2i-1)})\\
&\quad + C_{1y}l_1(\dot{y}_{ti} + l_1\dot{\varphi}_{ti} - h_4\dot{\theta}_{ti} - \dot{y}_{w(2i-1)}) - K_{1y}l_1(y_{ti} - l_1\varphi_{ti} - h_4\theta_{ti} - y_{w(2i)})\\
&\quad - C_{1y}l_1(\dot{y}_{ti} - l_1\dot{\varphi}_{ti} - h_4\dot{\theta}_{ti} - \dot{y}_{w(2i)}) + K_{1x}b_1^2(\varphi_{ti} - \varphi_{w(2i-1)}) + C_{1x}b_1^2(\dot{\varphi}_{ti} - \dot{\varphi}_{w(2i-1)})\\
&\quad + K_{1x}b_1^2(\varphi_{ti} - \varphi_{w(2i)}) + C_{1x}b_1^2(\dot{\varphi}_{ti} - \dot{\varphi}_{w(2i)}) = 0
\end{aligned} \tag{5}
$$

$$
\begin{aligned}
&J_{tx}\ddot{\theta}_{ti} - K_{2y}h_3(y_c - (-1)^i l\varphi_c - h_1\theta_c - y_{ti} - h_3\theta_{ti})\\
&\quad - C_{2y}h_5(\dot{y}_c - (-1)^i l\dot{\varphi}_c - h_2\dot{\theta}_c - \dot{y}_{ti} - h_5\dot{\theta}_{ti})\\
&\quad - K_{2z}b_2^2(\theta_c - \theta_{ti}) - C_{2z}b_3^2(\dot{\theta}_c - \dot{\theta}_{ti}) - K_{1y}h_4(y_{ti} + l_1\varphi_{ti} - h_4\theta_{ti} - y_{w(2i-1)})\\
&\quad - C_{1y}h_4(\dot{y}_{ti} - l_1\dot{\varphi}_{ti} - h_4\dot{\theta}_{ti} - \dot{y}_{w(2i-1)}) - K_{1y}h_4(y_{ti} - l_1\varphi_{ti} - h_4\theta_{ti} - y_{w(2i)})\\
&\quad - C_{1y}h_4(\dot{y}_{ti} - l_1\dot{\varphi}_{ti} - h_4\dot{\theta}_{ti} - \dot{y}_{w(2i)}) + 2K_{1z}b_1^2\theta_{ti} + 2C_{1z}b_1^2\dot{\theta}_{ti} = -u_i h_5
\end{aligned} \tag{6}
$$

(c) *Wheelset dynamics* ($i = 1 \sim 2$ *while* $j = 1$, $i = 3 \sim 4$ *while* $j = 2$):

$$
\begin{aligned}
&M_w\ddot{y}_{wi} - K_{1y}(y_{tj} - (-1)^i l_1\varphi_{tj} - h_4\theta_{tj} - y_{wi}) - C_{1y}(\dot{y}_{tj} - (-1)^i l_1\dot{\varphi}_{tj} - h_4\dot{\theta}_{tj} - \dot{y}_{wi})\\
&\quad + 2f_{22}\left[\frac{\dot{y}_{wi}}{V}\left(1 + \frac{\sigma r_0}{b}\right) - \varphi_{wi}\right] + K_{gy}y_{wi} = 2f_{22}\left(\frac{\sigma r_0}{Vb}\dot{y}_{ai} + \frac{\sigma r_0^2}{Vb}\dot{\theta}_{cli}\right)\\
&\quad + K_{gy}(y_{ai} + r_0\theta_{cli})
\end{aligned} \tag{7}
$$

$$
J_{wz}\ddot{\varphi}_{wi} + K_{1x}b_1^2(\varphi_{wi} - \varphi_{tj}) + 2f_{11}\left(\frac{b\lambda_e}{r_0}y_{wi} + \frac{b^2}{V}\dot{\varphi}_{wi}\right) - K_{g\varphi}\varphi_{wi} = 2f_{11}\frac{b\lambda_e}{r_0}(y_{ai} + r_0\theta_{cli}), \tag{8}
$$

where K_{gy} is the lateral gravitational stiffness and $K_{g\varphi}$ is the yaw gravitational stiffness, which are given by [37]

$$
K_{gy} = \frac{W\lambda_e}{b}, \tag{9}
$$

$$
K_{g\varphi} = -Wb\lambda_e. \tag{10}
$$

The other symbols in Equations (1)–(10) are defined in Table A1.

Let $\mathbf{q}$ be defined as the following vector:

$$
\mathbf{q} = [y_c\ \ \varphi_c\ \ \theta_c\ \ y_{t1}\ \ \varphi_{t1}\ \ \theta_{t1}\ \ y_{t2}\ \ \varphi_{t2}\ \ \theta_{t2}\ \ y_{w1}\ \ \varphi_{w1}\ \ y_{w2}\ \ \varphi_{w2}\ \ y_{w3}\ \ \varphi_{w3}\ \ y_{w4}\ \ \varphi_{w4}]^T,
$$

then the governing equations (1)–(10) can be rewritten in the following matrix form:

$$
\mathbf{M}\ddot{\mathbf{q}} + \mathbf{C}\dot{\mathbf{q}} + \mathbf{K}\mathbf{q} = \mathbf{F}_\mathbf{u}\mathbf{u} + \mathbf{F}_\mathbf{w}\mathbf{w}, \tag{11}
$$

where $\mathbf{M}(\in \mathbf{R}^{17\times17})$, $\mathbf{C}(\in \mathbf{R}^{17\times17})$, and $\mathbf{K}(\in \mathbf{R}^{17\times17})$ are the mass, damping, and stiffness matrixes of the train system; $\mathbf{u}(=[u_1\ u_2]^{\mathrm{T}})$ is the vector of the damping forces generated by the MR dampers; $\mathbf{w}(\in \mathbf{R}^{16\times1})$ is the vector that represents the track irregularities functioned on the wheels of the wheelsets; and $\mathbf{F_u}(\in \mathbf{R}^{17\times2})$ and $\mathbf{F_w}(\in \mathbf{R}^{17\times16})$ are the coefficient matrixes that are related to the installation of the MR dampers and the track irregularities.

Let $\mathbf{w} = [\mathbf{w_1}\ \mathbf{w_2}]^{\mathrm{T}}$, then $\mathbf{w_1}$ and $\mathbf{w_2}$, which will be defined in Section 2.2, can be expressed as

$$\mathbf{w_1} = [y_{a1}\ \ y_{a2}\ \ y_{a3}\ \ y_{a4}\ \ \theta_{cl1}\ \ \theta_{cl2}\ \ \theta_{cl3}\ \ \theta_{cl4}]^{\mathrm{T}}, \tag{12}$$

$$\mathbf{w_2} = [\dot{y}_{a1}\ \ \dot{y}_{a2}\ \ \dot{y}_{a3}\ \ \dot{y}_{a4}\ \ \dot{\theta}_{cl1}\ \ \dot{\theta}_{cl2}\ \ \dot{\theta}_{cl3}\ \ \dot{\theta}_{cl4}]^{\mathrm{T}}. \tag{13}$$

According to Equations (1)–(10)and the definitions of the vectors **q**, **u**, and **w**, the coefficient matrixes in Equation (11) can be determined.

2.2. *Random track irregularities*

Track geometrical variations are the primary causes of the vibrations of the railway vehicles. The geometrical track irregularities include the vertical profile, cross-level, lateral alignment, and gauge irregularities [37]. The lateral vibration of the train system is mainly induced by the lateral alignment (y_a) and cross-level (θ_{cl}) of the track irregularities (Figure 2), which can be expressed as [38,39]

$$y_a = \frac{y_l + y_r}{2}, \quad \theta_{cl} = \frac{z_l - z_r}{2b}, \tag{14}$$

where y_l and y_r represent the lateral track irregularities of the left and right rail, respectively; z_l and z_r represent the vertical track irregularities of the left and right rail, respectively.

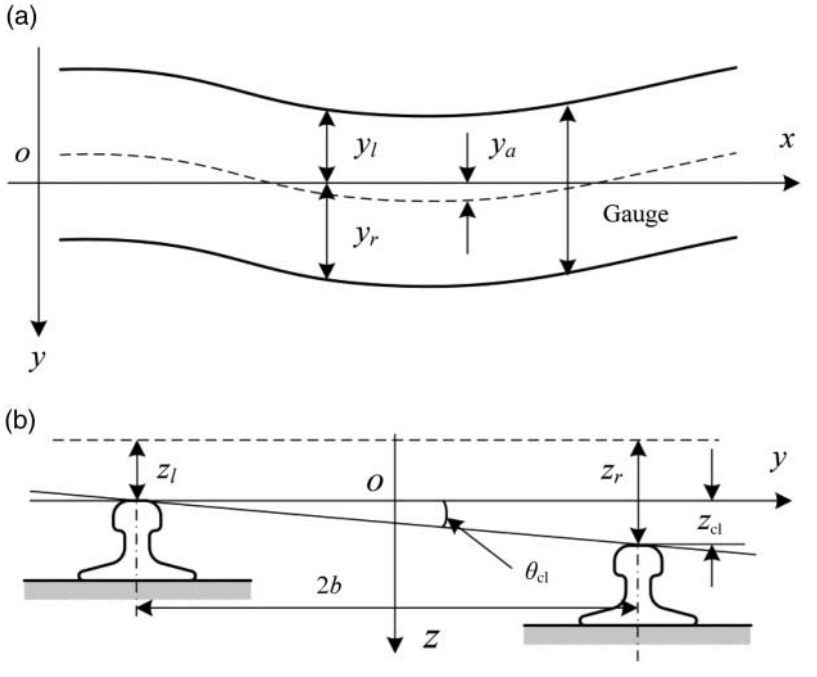

Figure 2. Definitions of the track irregularities: (a) the lateral alignment and gauge and (b) the vertical profile and cross level.

The random track irregularities are usually described by their power spectral densities (PSDs), which are determined from the measured data. The one-sided density functions of the lateral alignment and cross-level are given by the following equations, respectively [40]:

$$S_a(\Omega) = \frac{A_a \Omega_c^2}{(\Omega^2 + \Omega_r^2)(\Omega^2 + \Omega_c^2)}, \tag{15}$$

$$S_c(\Omega) = \frac{(A_v/b^2)\Omega_c^2 \Omega^2}{(\Omega^2 + \Omega_r^2)(\Omega^2 + \Omega_c^2)(\Omega^2 + \Omega_s^2)}, \tag{16}$$

where Ω is the spatial frequency (rad/m); Ω_c, Ω_r, and Ω_s are truncated wavenumbers (rad/m); b is the half of the reference distance between the rails; and A_a and A_v are scalar factors of the track irregularities [40]. The values of the constants are listed in Table A1.

The PSD functions of the lateral alignment and cross-level can be rewritten as follows:

$$S_a(\omega) = \frac{AV^3\Omega_c^2}{(\omega^2 + (V\Omega_r)^2)(\omega^2 + (V\Omega_c)^2)}, \tag{17}$$

$$S_c(\omega) = \frac{(A/b^2)V^3\Omega_c^2\omega^2}{(\omega^2 + (V\Omega_r)^2)(\omega^2 + (V\Omega_c)^2)(\omega^2 + (V\Omega_s)^2)}, \tag{18}$$

where V is the train velocity and ω equal to $V\Omega$ is the angular frequency.

The frequency domain method, proposed by Guo and Ming [41], is used to calculate the track irregularity in time domain. The main processes of the method are as follows: First, change the unilateral PSD function of the track irregularity into bilateral function. Then calculate discrete samples of the bilateral function through discrete sampling processing. Third calculate the frequency spectrum of the track irregularity on the basis of the sampling results and random phases. Lastly implement inverse fast Fourier transform for the frequency spectrum and obtain the time series of the track irregularity. Figures 3 and 4 show the time series of the lateral alignment and the cross-level of the track irregularity, respectively. From Figures 3(b) and 4(b), it can be found that the PSDs of the simulated time series agree well with the analytic solution.

3. Dynamics of MR fluid dampers

3.1. *Foreword dynamics of MR fluid dampers*

The prototype MR damper used in this study was designed and manufactured by our group (Figure 5). The damper has a ±57 mm stroke with 510 mm length in its extended posi-

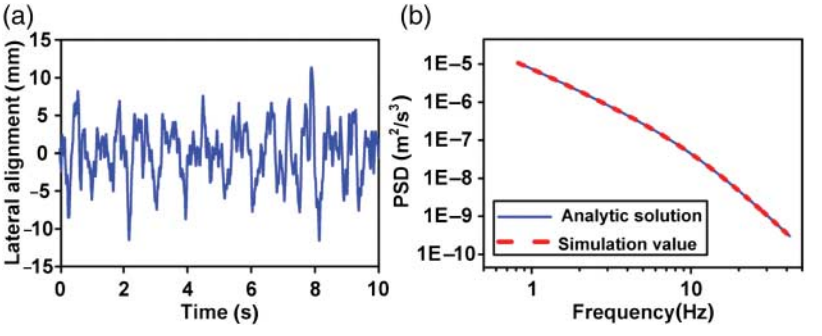

Figure 3. Time series of the lateral alignment of the track irregularity: (a) time series and (b) comparison of the PSD of analytic solution and simulation value.

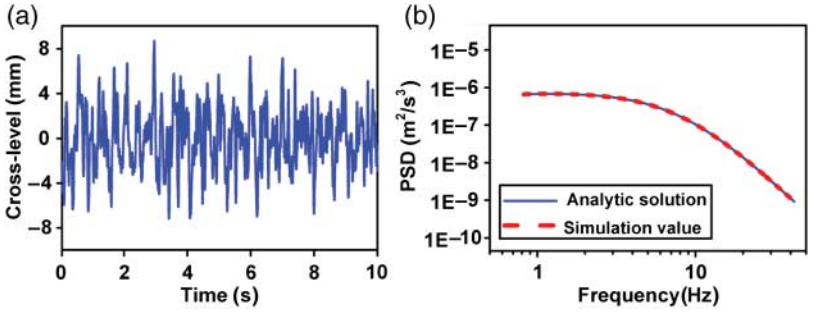

Figure 4. Time series of the cross-level of the track irregularity: (a) time series and (b) comparison of the PSD of analytic solution and simulation value.

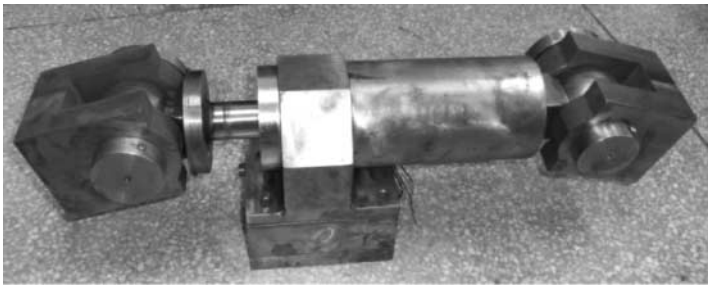

Figure 5. Photograph of the MR damper.

tion and 396 mm length in its compressed position. The maximum input current to the MR damper is 1.2 A.

The MTS809 TestStar Material Testing System is used to test the MR damper. In each test, the excitation is a sinusoidal-varying displacement of fixed frequency and amplitude, and the input current to the MR damper is maintained at a constant level. The displacement amplitudes are 15, 20 and 25 mm when the excitation frequency is 1 Hz. While the excitation frequency is 2 Hz, the displacement amplitudes are 10, 15 and 20 mm, respectively. The applied input current are from 0 to 1.2 A with increment of 0.2 A. The damping force and displacement are measured and fed to a computer. The velocity is obtained by differentiating the displacement.

The phenomenological model, proposed by Spencer *et al*. [25], can accurately predict the behaviour of the MR damper over a broad range of inputs. Considering there is no gas accumulator in the prototype used for trains, the spring terms in the phenomenological model could be ignored. Thus, a modified Bouc–Wen model (Figure 6) is proposed based on the phenomenological model, which is described by the following five nonlinear differential equations (19)–(23):

$$F = c_1\dot{y}, \tag{19}$$

$$\dot{y} = \frac{1}{c_0 + c_1}[\alpha z + c_0\dot{x}], \tag{20}$$

$$\dot{z} = -\gamma|\dot{x} - \dot{y}|z|z|^{n-1} - \beta(\dot{x} - \dot{y})|z|^n + A(\dot{x} - \dot{y}), \tag{21}$$

where F is the damping force; c_1 represents the viscous damping at low velocities; c_0 represents the viscous damping at high velocities; x is the piston relative displacement; y is the internal displacement and z is the evolutionary variable; α is a scaling value for the Bouc–Wen

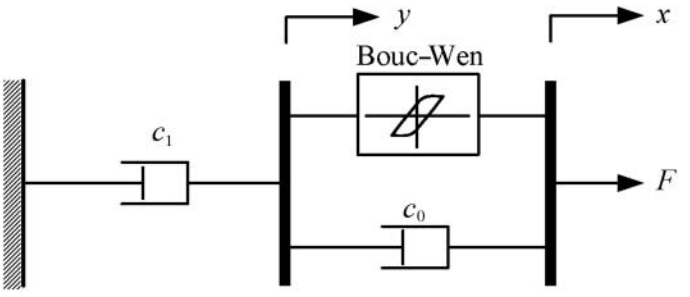

Figure 6. Schematic of the modified Bouc–Wen model for the MR damper.

hysteresis loop; and γ, β, A, and n are parameters used to adjust the scale and shape of the hysteresis loop.

The parameters γ, β, A, n, and c_1 are considered as constants, and the parameters c_0 and α are assumed to be functions of the applied current I as follows:

$$\alpha = \alpha_a + \alpha_b I + \alpha_c I^2, \tag{22}$$

$$c_0 = c_{0a} + c_{0b} I. \tag{23}$$

Eventually, there are 10 parameters c_{0a}, c_{0b}, α_a, α_b, α_c, c_1, γ, β, A, and n for the modified Bouc–Wen model. The experimental data of 1 Hz frequency at 20 mm amplitude of excitation and every single input current are used to estimate the parameters. The assessment criterion is the error between the model predicted force (F_p) and the experimental force (F_e) over one complete cycle. The error in the model is represented by the objective function E_t, which is given by

$$E_t = \frac{\xi_t}{\sigma_F}, \tag{24}$$

$$\xi_t^2 = \int_0^T (F_e - F_p)^2 \, dt, \tag{25}$$

$$\sigma_F^2 = \int_0^T (F_e - \mu_F)^2 \, dt, \tag{26}$$

where μ_F is the average value of the force obtained in experiment (F_e) over one complete cycle. Optimum values of the 10 parameters have been obtained using genetic algorithm tool available in MATLAB® Toolboxes. The optimum values are listed in Table 2.

In order to validate the obtained modified Bouc–Wen model, the measured damping force and the predicted damping force are compared (Figure 7), where the excitation condition is 1 Hz frequency, ±20 mm amplitude and 2 Hz frequency, ±15 mm amplitude, respectively. It

Table 2. Parameter values of the modified Bouc–Wen model.

Parameter	Values	Parameter	Values
C_{0a}	8.4 N s mm^{-1}	c_1	91.6 N s mm^{-1}
C_{0b}	11.23 N s mm^{-1} A^{-1}	β	0.15 mm^{-2}
α_a	40 N mm^{-1}	A	4.5
α_b	2036.8 N mm^{-1} A^{-1}	γ	0.15 mm^{-2}
α_c	−535.95 N mm^{-1} A^{-2}	n	2

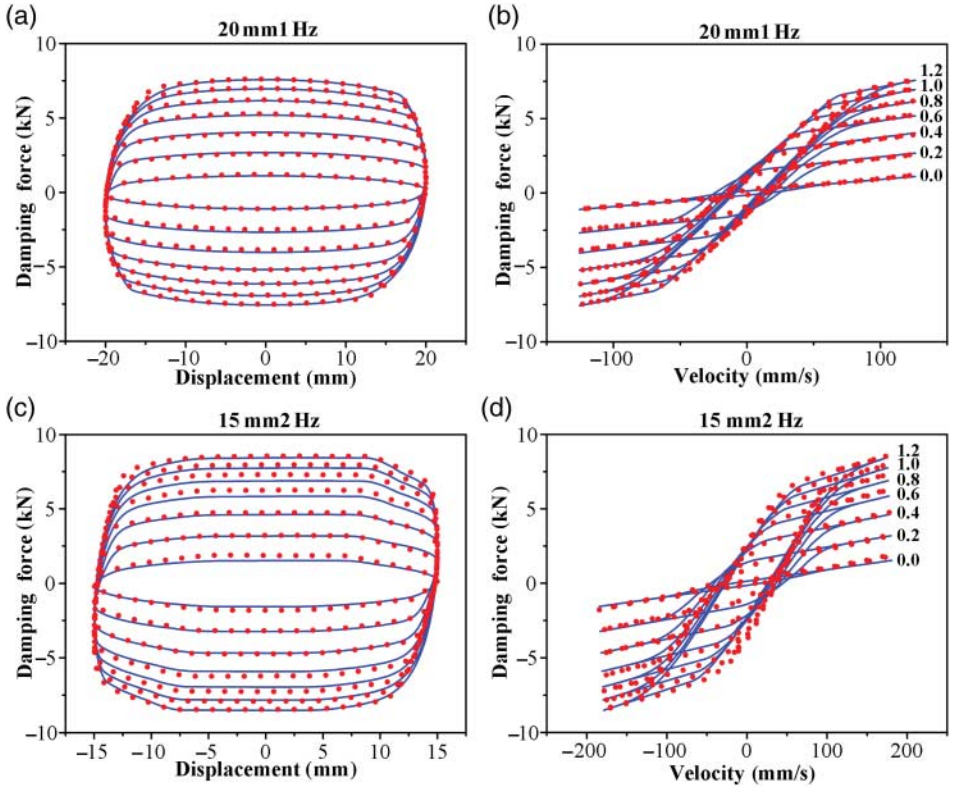

Figure 7. Comparison of the modified Bouc–Wen model predicted results and experimental results: (a) force versus displacement (1 Hz, ±20 mm); (b) force versus velocity (1 Hz, ±20 mm); (c) force versus displacement (2 Hz, ±15 mm); and (d) force versus velocity (2 Hz, ±15 mm).

is clearly observed that the damping forces predicted by the modified Bouc–Wen model agree well with the experimental forces, which indicates that the mode can accurately describe the forward dynamics of the prototype damper and can be used in simulations.

3.2. *Inverse dynamics of MR fluid dampers*

3.2.1. *Training of the inverse model*

Inverse MR damper models are used to obtain the command current according to the desired force in actual application. In this section, the ANFIS technique, which possesses universal approximation ability to nonlinear system [42], is applied to build the inverse MR damper model. As an example, Figure 8 illustrates the architecture of a two-input two-rule ANFIS [42]. The ANFIS contains five layers. Each layer carries out one kind of calculation and the node functions in the same layer are of the same function family.

Given input/output data sets, ANFIS constructs fuzzy inference system whose membership function parameters are adjusted using a hybrid algorithm. Generally speaking, with increasing number of the input date sets, the accuracy of the inverse model increases. However, the inverse model will become very complex and the training time will increase enormously. To balance the model accuracy and time consumption, the inputs of the inverse model are chosen as current velocity, previous velocity, velocity before previous moment, current desired damping force, and previous desired damping force, while the output is the current command current.

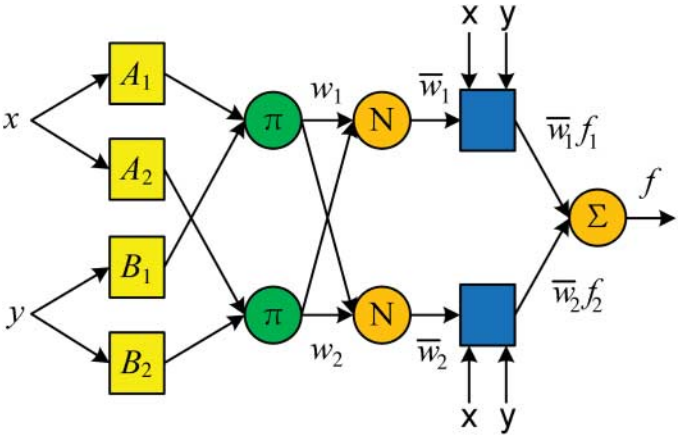

Figure 8. Architecture of a two-input two-rule ANFIS.

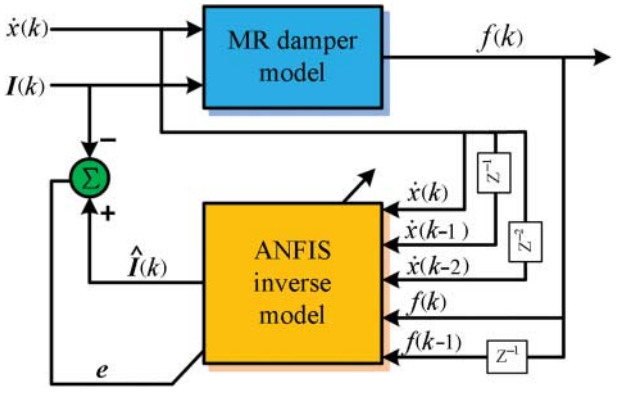

Figure 9. Scheme of the ANFIS for modelling the inverse dynamics of the MR damper.

Figure 9 shows the scheme of the ANFIS for modelling the inverse dynamics of the MR damper. The velocity input is a Gaussian white noise signal with frequency between 0 and 3 Hz and amplitude ±40 mm. The command input current is generated by Gaussian white noise ranging from 0 to 1 A with frequency 0–3 Hz. The desired damping force is produced by the modified Bouc–Wen model, which is built in Section 3.1, according to the displacement and command current inputs. The data are collected for 20 s and sampled at 1000 Hz, so 20,000 points of data are generated. The first 10,000 points of data are chosen to be the training data while the later 10,000 points of data are used as checking data.

3.2.2. *Validation of the inverse model*

Three data sets are discussed to valid the inverse dynamic neuro-fuzzy model. The first and second validation case is the training data and the checking data, respectively. The third validation case is the application of the ANFIS model in semi-active control for train suspension system, which will be discussed in the Section 6. The training data validation case is shown in Figure 10. It can be found that the predicted command current can track the target command current reasonably well from Figure 10(a), and the damping force produced by the predicted

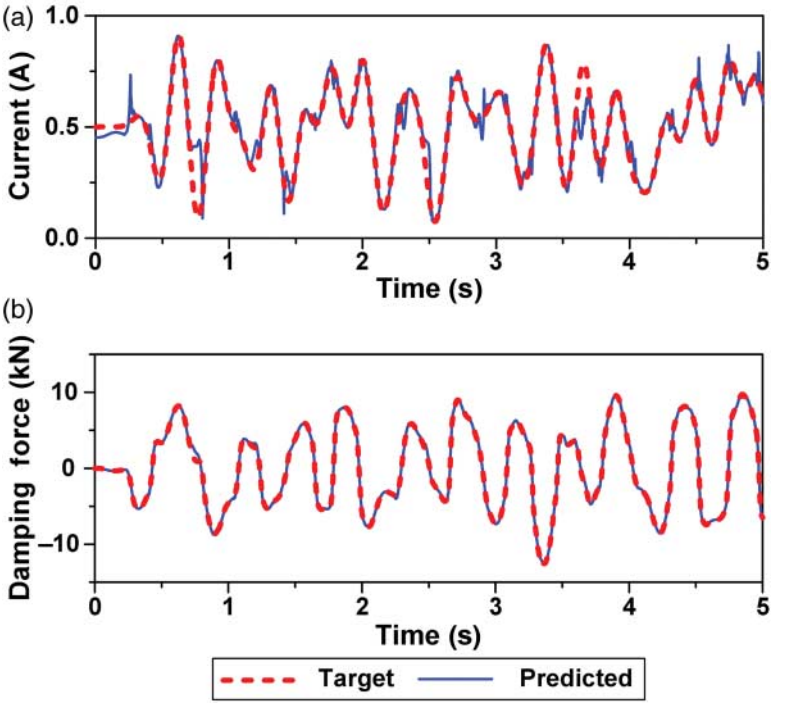

Figure 10. Validation of the ANFIS inverse model of the MR damper for training data: (a) the command current predicted by the ANFIS model and (b) the force predicted from the command current.

command current coincides well with the damping force produced by the target command current from Figure 10(b).

The checking data validation case is shown in Figure 11. From Figure 11(a), it can be found that the accuracy of checking data is not as good as that of training data. Fortunately, from Figure 11(b) we can see that the damping force generated by the predicted command current can track the damping force generated by the target command current well. This indicates that the inverse model of MR damper can satisfy the needs of applications, because the inverse model is mainly used to track the desired damping force.

4. Semi-active controller design

4.1. *Schematic of the MR damper-based semi-active control system*

The semi-active control system integrated with MR dampers consists of a system controller and a damper controller. The system controller generates the desired damping force according to the dynamic responses of the suspension, and the damper controller adjusts the input current to track the desired damping force. In this study, an MR damper-based semi-active H∞ controller for the railway vehicle suspension is proposed. This controller is made up of a H∞ controller (system controller) and ANFIS inverse MR damper models (damper controller). The structure of the semi-active controller for railway vehicle suspensions with MR dampers is depicted in Figure 12. First, the active control forces are calculated by the H∞ controllers according to the measured outputs. Then, the desired damping forces are generated by the force limiters based on the active control forces. Third, the ANFIS inverse

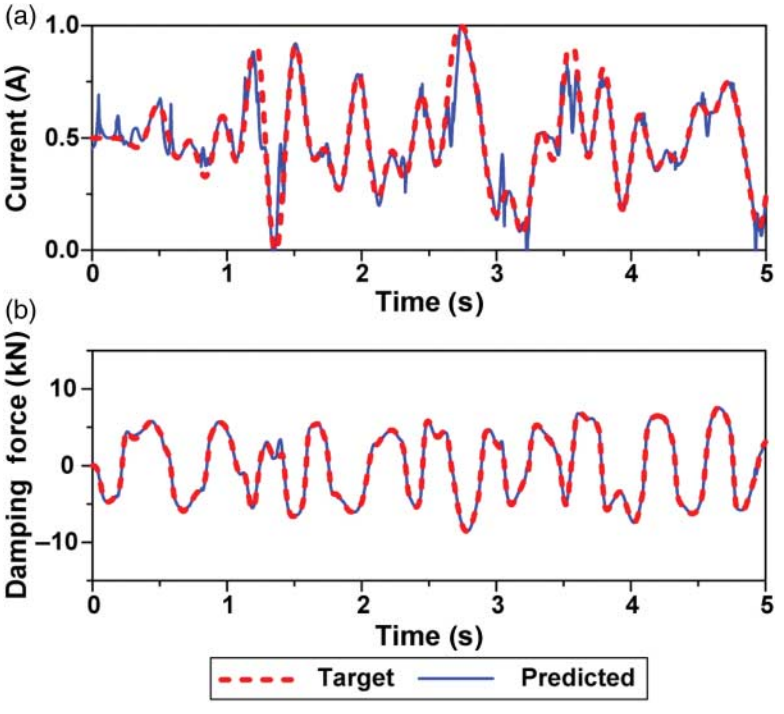

Figure 11. Validation of the ANFIS inverse model of the MR damper for checking data: (a) the command current predicted by the ANFIS model and (b) the force predicted from the command current.

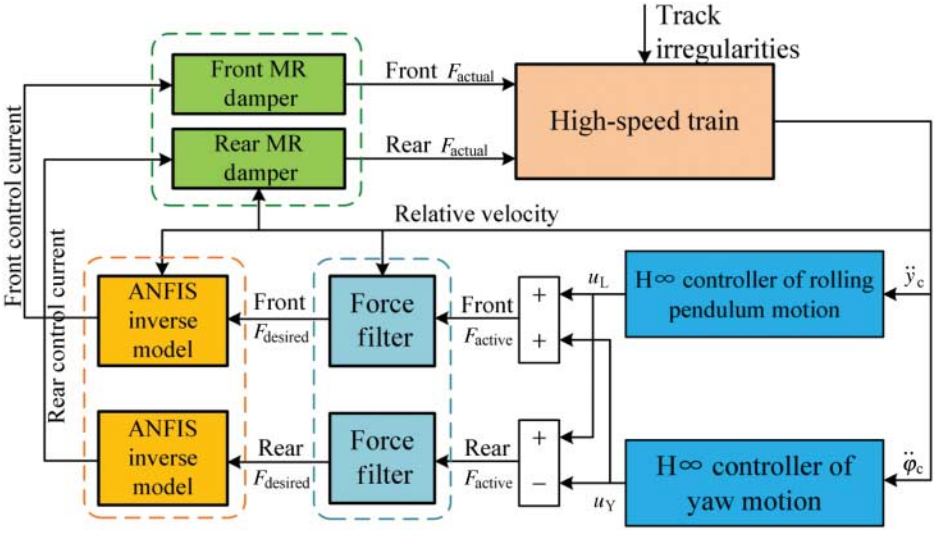

Figure 12. Structure of the semi-active controller for railway vehicle suspension with MR dampers.

models of MR dampers adjust the command currents according to the desired damping force and the vehicle suspension responses. Finally, the desired damping forces are approximately realised by MR dampers with appropriate input currents calculated by the ANFIS inverse models.

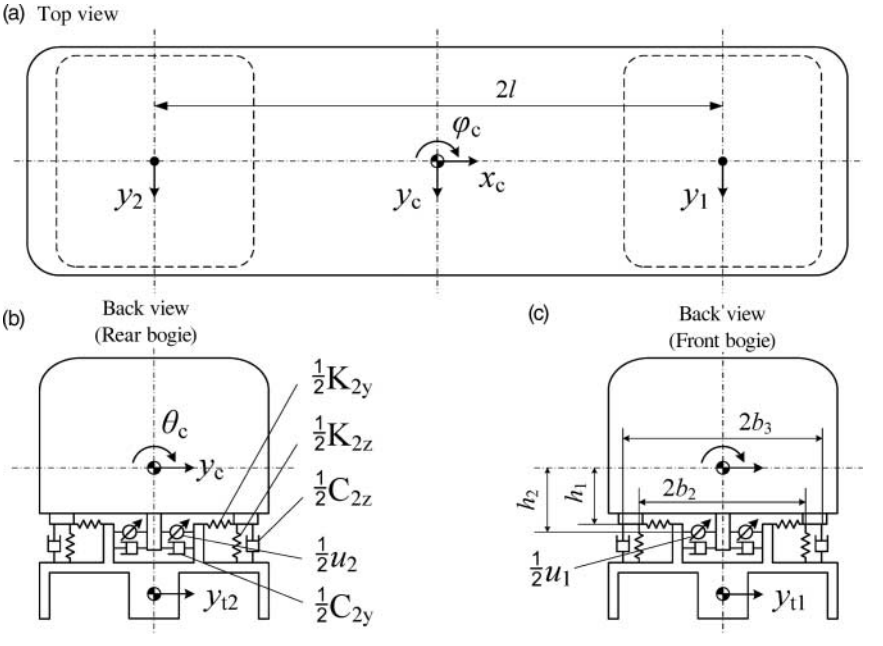

Figure 13. Lateral control model of the car body for the railway vehicle.

4.2. *System controller based on H∞ control law*

With faster speed and lighter bodies introduced to the high-speed train, the controller should be designed to be more robust. H∞ control has been proved a successful and thorough way to solve the robust control problem. Thus, in this section the H∞ control is adopted to establish the system controller to attenuate the lateral vibration of the high-speed train.

In practical applications, it is important to build a simplified control model, which can reveal the influence from the controller to the controlled system but does not contain all of the details, because more complex control model will induce a more complex controller. Figure 13 shows the lateral control model of the railway vehicle, which contains the lateral, yaw, and roll motion of the car body [43]. This model only considers the lateral motion of the car body with secondary suspension, because the vertical motion and lateral motion of the railway vehicle are relatively independent [37]. The governing equations of the control model are presented as follows.

Car body lateral motion:

$$M_c\ddot{y}_c + K_{2y}(y_c + l\varphi_c - h_1\theta_c - y_{t1}) + C_{2y}(\dot{y}_c + l\dot{\varphi}_c - h_2\dot{\theta}_c - \dot{y}_{t1}) + K_{2y}(y_c - l\varphi_c - h_1\theta_c - y_{t2}) + C_{2y}(\dot{y}_c - l\dot{\varphi}_c - h_2\dot{\theta}_c - \dot{y}_{t2}) = u_1 + u_2. \quad (27)$$

Car body yaw motion:

$$J_{cz}\ddot{\varphi}_c + K_{2y}l(y_c + l\varphi_c - h_1\theta_c - y_{t1}) + C_{2y}l(\dot{y}_c + l\dot{\varphi}_c - h_2\dot{\theta}_c - \dot{y}_{t1}) - K_{2y}l(y_c - l\varphi_c - h_1\theta_c - y_{t2}) - C_{2y}l(\dot{y}_c - l\dot{\varphi}_c - h_2\dot{\theta}_c - \dot{y}_{t2}) = u_1 l - u_2 l. \quad (28)$$

Car body roll motion:

$$\begin{aligned} J_{cx}\ddot{\theta}_c - K_{2y}h_1(y_c + l\varphi_c - h_1\theta_c - y_{t1}) - C_{2y}h_2(\dot{y}_c + l\dot{\varphi}_c - h_2\dot{\theta}_c - \dot{y}_{t1}) \\ - K_{2y}h_1(y_c - l\varphi_c - h_1\theta_c - y_{t2}) - C_{2y}h_2(\dot{y}_c - l\dot{\varphi}_c - h_2\dot{\theta}_c - \dot{y}_{t2}) \\ + 2K_{2z}b_2^2\theta_c + 2C_{2z}b_3^2\dot{\theta}_c = -u_1h_2 - u_2h_2. \end{aligned} \tag{29}$$

Assume that the lateral displacements of the connection points on the car body between the car body and the MR dampers are y_1 and y_2 (Figure 13), where y_1 represents the lateral displacement of the front connection point on the car body and y_2 represents the lateral displacement of the rear connection point on the car body, respectively. The lateral (y_c) and yaw (φ_c) motions of the car body can be rewritten as follows:

$$y_c = \frac{y_1 + y_2}{2}, \quad \varphi_c = \frac{y_1 - y_2}{2l}. \tag{30}$$

Moreover, it is also important to choose appropriate weight function to optimise all aspects of performance of the controller. More complex control model contains more controlled variables, then the choice of the weight functions for all controlled variables will become more difficult. For this reason, the H∞ controller is further simplified and divided into two parts, including the controller of the yaw motion and the controller of the rolling pendulum motion (lateral motion + roll motion). The two controllers can be established separately because the lateral and yaw motions are not strongly coupled.

(a) *$H\infty$ controller of the yaw motion*

Pertaining to the yaw motion of the car body, define: $y_{Yc} = (y_1 - y_2)/2, y_{Yt} = (y_{t1} - y_{t2})/2$, $\Delta y_Y = y_{Yc} - y_{Yt}, u_Y = (u_1 - u_2)/2$, where y_{t1} and y_{t2} represent the displacements of the front bogie and rear bogie, respectively. u_1 and u_2 represent the front and rear control force generated by the MR dampers. The system variable of the controller x_Y is defined as $x_Y = [\dot{y}_{Yc}, \Delta y_Y]^T$ and the evaluation vector is chosen as $z_Y = [\ddot{y}_{Yc}, u_Y]^T$. The measurement output is $y_Y = \ddot{y}_{Yc}$ and the disturbance input is $w_Y = \dot{y}_{Yt}$. Then the yaw H∞ controller can be written in state-space form as

$$\begin{aligned} \dot{x}_Y &= A_Y x_Y + B_{1Y} w_Y + B_{2Y} u_Y, \\ z_Y &= C_{1Y} x_Y + D_{11Y} w_Y + D_{12Y} u_Y, \\ y_Y &= C_{2Y} x_Y + D_{21Y} w_Y + D_{22Y} u_Y, \end{aligned} \tag{31}$$

where

$$A_Y = \begin{bmatrix} -2C_{2y}l^2/J_{cz} & -2K_{2y}l^2/J_{cz} \\ 1 & 0 \end{bmatrix}, \quad B_{1Y} = \begin{bmatrix} 2C_{2y}l^2/J_{cz} \\ -1 \end{bmatrix}, \quad B_{2Y} = \begin{bmatrix} l^2/J_{cz} \\ 0 \end{bmatrix},$$

$$C_{1Y} = \begin{bmatrix} -2C_{2y}l^2/J_{cz} & -2K_{2y}l^2/J_{cz} \\ 0 & 0 \end{bmatrix}, \quad D_{11Y} = \begin{bmatrix} 2C_{2y}l^2/J_{cz} \\ 0 \end{bmatrix}, \quad D_{12Y} = \begin{bmatrix} l^2/J_{cz} \\ 1 \end{bmatrix},$$

$$C_{2Y} = \begin{bmatrix} -2C_{2y}l^2/J_{cz} & -2K_{2y}l^2/J_{cz} \end{bmatrix}, \quad D_{11Y} = \begin{bmatrix} 2C_{2y}l^2/J_{cz} \end{bmatrix}, \quad D_{12Y} = \begin{bmatrix} l^2/J_{cz} \end{bmatrix}.$$

The design objective of the controller is aimed to suppress the lateral vibration of the car body in the very frequency range where the influence on the ride comfort is the greatest; at the same time avoiding the frequency band of the control force to be too wide. The frequency range of the vibration with the biggest impact on the ride comfort is 0.5–10 Hz, so a band-pass transfer function $\alpha_{Y_y} W_{Y_y}(s)$ ranging from 0.1 to 10 Hz, centring at 0.8 Hz (approximate natural frequency of the car body) is introduced to weight $\ddot{y}_Y$. The control force with high

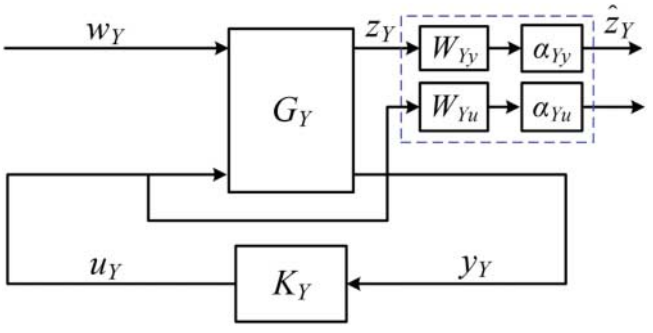

Figure 14. Design structure of H∞ controller of the yaw motion.

frequency could not be easily tracked by an MR damper because of the time delay, thus a low-pass transfer function $\alpha_{\mathrm{Y}u}W_{\mathrm{Y}u}(\mathrm{s})$ is introduced to weight u_{Y}, which would decrease the control force up 10 Hz. The design structure is shown in Figure 14, where G_{Y} is the yaw motion system of the car body, K_{Y} is the H∞ controller of the yaw motion, $W_{\mathrm{Y}y}(\mathrm{s})$ and $W_{\mathrm{Y}u}(\mathrm{s})$ are the transfer functions with static gain equal to 1, and $\alpha_{\mathrm{Y}y}$ and $\alpha_{\mathrm{Y}u}$ are the static gains of the transfer functions

$$\alpha_{\mathrm{Y}y} = 1, \quad W_{\mathrm{Y}y} = \frac{s^2 + 1.17s + 25}{s^2 + 15.54s + 25}, \tag{32}$$

$$\alpha_{\mathrm{Y}u} = 1 \times 10^{-6}, \quad W_{\mathrm{Y}u} = \frac{s^2 + 132s + 507,400}{20s^2 + 3532s + 507,400}. \tag{33}$$

(b) *H∞ controller of the rolling pendulum motion*

For the rolling pendulum motion of the car body, define: $y_{\mathrm{Lc}} = (y_1 + y_2)/2$, $y_{\mathrm{Lt}} = (y_{\mathrm{t}1} + y_{\mathrm{t}2})/2$, $\Delta y_{\mathrm{L}} = y_{\mathrm{Lc}} - y_{\mathrm{Lt}}$, $u_{\mathrm{L}} = (u_1 + u_2)/2$. The system variable of the controller x_{L} is defined as $x_{\mathrm{L}} = [\dot{y}_{\mathrm{c}}, \Delta y_{\mathrm{L}}, \dot{\theta}_{\mathrm{c}}, \theta_{\mathrm{c}}]^{\mathrm{T}}$ and the evaluation vector is chosen as $z_{\mathrm{L}} = [\ddot{y}_{\mathrm{Lc}}, u_{\mathrm{L}}]^{\mathrm{T}}$. The measurement output is $y_{\mathrm{L}} = \ddot{y}_{\mathrm{Lc}}$ and the disturbance input is $w_{\mathrm{L}} = \dot{y}_{\mathrm{Lt}}$. Then the rolling pendulum H∞ controller can be written in state-space form as

$$\begin{aligned} \dot{x}_{\mathrm{L}} &= A_{\mathrm{L}}x_{\mathrm{L}} + B_{1\mathrm{L}}w_{\mathrm{L}} + B_{2\mathrm{L}}u_{\mathrm{L}}, \\ z_{\mathrm{L}} &= C_{1\mathrm{L}}x_{\mathrm{L}} + D_{11\mathrm{L}}w_{\mathrm{L}} + D_{12\mathrm{L}}u_{\mathrm{L}}, \\ y_{\mathrm{L}} &= C_{2\mathrm{L}}x_{\mathrm{L}} + D_{21\mathrm{L}}w_{\mathrm{L}} + D_{22\mathrm{L}}u_{\mathrm{L}}, \end{aligned} \tag{34}$$

where

$$A_{\mathrm{L}} = \begin{bmatrix} -2C_{2y}/M_{\mathrm{c}} & -2K_{2y}/M_{\mathrm{c}} & 2C_{2y}h_2/M_{\mathrm{c}} & 2K_{2y}h_1/M_{\mathrm{c}} \\ 1 & 0 & 0 & 0 \\ 2C_{2y}h_2/J_{cx} & 2K_{2y}h_1/J_{cx} & 2(C_{2y}h_2^2 + C_{2z}b_3^2)/J_{cx} & 2(K_{2y}h_1^2 + K_{2z}b_2^2)/J_{cx} \\ 0 & 0 & 1 & 0 \end{bmatrix},$$

$$B_{1\mathrm{L}} = \begin{bmatrix} 2C_{2y}/M_{\mathrm{c}} \\ -1 \\ -2C_{2y}h_2/J_{cx} \\ 0 \end{bmatrix}, \quad B_{2\mathrm{L}} = \begin{bmatrix} 2/M_{\mathrm{c}} \\ 0 \\ -2h_2/J_{cx} \\ 0 \end{bmatrix},$$

$$C_{1\mathrm{L}} = \begin{bmatrix} -2C_{2y}/M_{\mathrm{c}} & -2K_{2y}/M_{\mathrm{c}} & 2C_{2y}h_2/M_{\mathrm{c}} & 2K_{2y}h_1/M_{\mathrm{c}} \\ 0 & 0 & 0 & 0 \end{bmatrix};$$

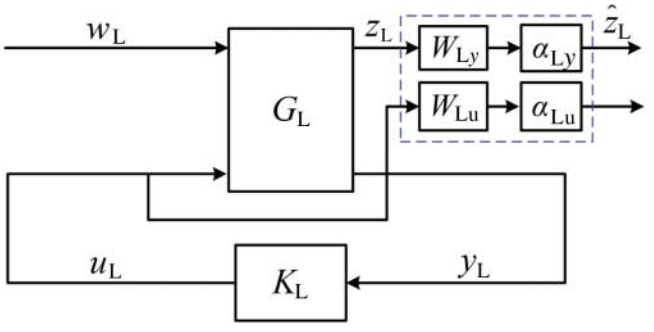

Figure 15. Design structure of H∞ controller of the rolling pendulum motion.

$$D_{11L} = \begin{bmatrix} 2C_{2y}/M_c \\ 0 \end{bmatrix}, \quad D_{12L} = \begin{bmatrix} 2/M_c \\ 1 \end{bmatrix},$$
$$C_{2L} = \begin{bmatrix} -2C_{2y}/M_c & -2K_{2y}/M_c & 2C_{2y}h_2/M_c & 2K_{2y}h_1/M_c \end{bmatrix};$$
$$D_{21L} = \begin{bmatrix} 2C_{2y}/M_c \end{bmatrix}, \quad D_{12L} = [2/M_c].$$

As stated previously, the frequency range of the vibration with the biggest impact on the ride comfort is 0.5–10 Hz, so a band-pass transfer function $\alpha_{Ly}W_{Ly}(s)$ ranging from 0.1 to 10 Hz, centring at 1 Hz (approximate natural frequency of the car body) is selected to weight $\ddot{y}_L$. A low-pass transfer function $\alpha_{Lu}W_{Lu}(s)$ is used to weight u_L in order to make the frequency of control force concentrate below 10 Hz. The design structure is shown in Figure 15, where G_L is the rolling pendulum motion system of the car body, K_Y is the H∞ controller of the rolling pendulum motion, $W_{Ly}(s)$ and $W_{Lu}(s)$ are the transfer functions with static gain equal to 1, and α_{Ly} and α_{Lu} are the static gains of the transfer functions

$$\alpha_{Ly} = 1, \quad W_{Ly} = \frac{s^2 + 2.77s + 23}{s^2 + 15.54s + 23}, \tag{35}$$

$$\alpha_{Lu} = 1 \times 10^{-6}, \quad W_{Lu} = \frac{s^2 + 132s + 507400}{20s^2 + 3532s + 507400}. \tag{36}$$

(c) *Integration*

The H∞ controller of the railway vehicle is composed of the yaw motion controller K_Y and the rolling pendulum motion controller K_L. The two controllers are independent and can be designed separately. The 'hinf' function in MATLAB® is used to calculate the H∞ controllers. The front control force u_1 and the rear control force u_2 can be expressed as

$$\begin{aligned} u_1 &= \frac{\alpha u_L + \beta u_Y}{2}, \\ u_2 &= \frac{\alpha u_L - \beta u_Y}{2}, \end{aligned} \tag{37}$$

where u_L is obtained by the rolling pendulum motion controller K_L and u_Y is obtained by the yaw motion controller K_Y. α and β are weighting coefficients of the u_L and u_Y, respectively. After comparing the control effects for a series of weighting values, the values are confirmed as $\alpha = 8$ and $\beta = 1$.

The inputs of the H∞ controller are the lateral accelerations of the connection points on the car body between the car body and the MR dampers, so two acceleration sensors are needed to measure these accelerations. The outputs of the controller are the front control force u_1 and the rear control force u_2, respectively.

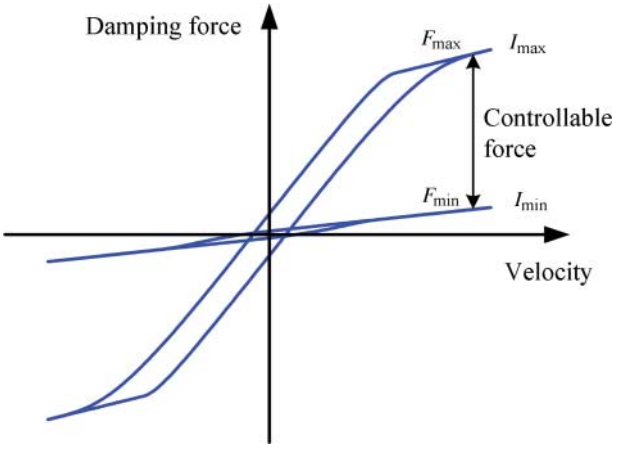

Figure 16. Schematic of the controllable force.

4.3. *Damper controller for MR damper-based semi-active systems*

From Equation (37), the active control forces of the railway vehicle can be determined. However, not all of these forces can be tracked by the MR dampers because of two intrinsic constraints: the passivity constraint and the limitation constraint (Figure 16). The damping force could be tracked by MR dampers only when the control force satisfies the two constraints. Otherwise, the damping force is set as either the lower or upper level by setting the input current at either zero or the maximum achievable level, respectively. Thus, a force limiter is designed to calculate the desired damping force according to the active control force and the suspension velocity, which is governed by

$$F_{\text{desired}} = \begin{cases} F_{\max}, & F_{\text{active}} \geq F_{\max}, \\ F_{\text{active}}, & F_{\max} > F_{\text{active}} > F_{\min} \\ F_{\min}, & F_{\text{active}} \leq F_{\min}, \end{cases} \tag{38}$$

where $F_{\max}$ and $F_{\min}$ are the maximum and minimum forces that can be generated by the MR damper at the present moment, respectively. F_{active} is the active control force calculated by the active control algorithm, F_{desired} is the desired damping force that can be tracked by the MR damper.

The ANFIS inverse models of the MR dampers (built in Section 3.2) are adopted to generate the command currents to track the desired damping forces. Both the Force Filter and the ANFIS inverse model need the MR damper's piston relative velocity. Hence anther two acceleration sensors are used to measure the lateral accelerations of the two bogies. Then the relative velocities can be obtained according to the measured outputs.

5. Simulation parameters

In order to evaluate the performance of the semi-active controller with MR dampers, two types of suspensions are considered, including passive and semi-active suspension. Passive suspension means the secondary suspension system of the railway vehicle is integrated with traditional

passive viscous dampers and the optimal damping coefficient is equal to 26,000 N s/m according to reference [44]. Semi-active suspension means that the secondary suspension system is integrated with MR dampers.

The structure of the full-scale railway vehicle model with 17 DOF is given in Figure 1. The symbols, their definitions, and parameter values of the full-scale railway vehicle model are listed in Table A1 [44]. The parameters for the MR dampers used in the simulations are given in Table 2. The H∞ controllers are calculated offline by adopting the 'hinf' function in MATLAB® and the parameter values are given in Section 4.2.

In the simulation, the 'Bogacki–Shampine' solver is adopted and a fixed time step size of 1e−5 is used. The time delay of the whole system is 50 ms and the total simulation time is 10 s.

6. Simulation results

6.1. *Car body accelerations*

In order to clarify the effects of the semi-active suspension system on the accelerations of the car body, the PSDs of the car body accelerations under the random track irregularities with the passive and semi-active suspension systems are shown in Figure 17. Their corresponding time histories are shown in Figure 18. The root-mean-square (RMS) and peak-to-peak values of the corresponding car body accelerations with the passive and semi-active suspension systems under the random track irregularities are given in Tables 3.

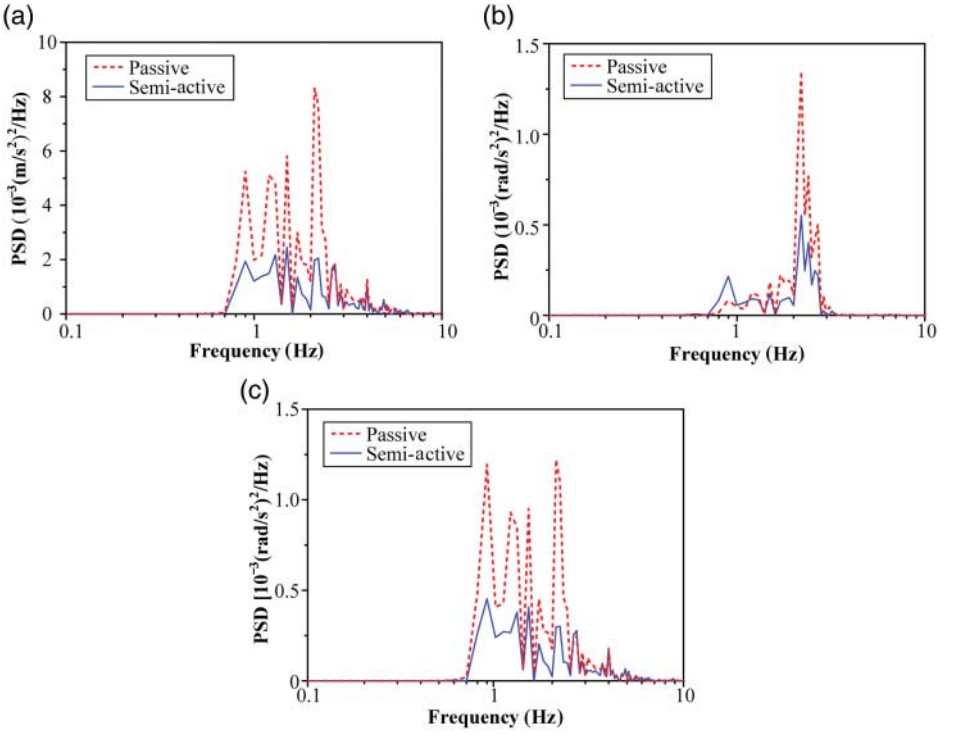

Figure 17. PSDs of the car body accelerations of the railway vehicles with different suspension systems under the random track irregularities: (a) lateral accelerations, (b) yaw accelerations, and (c) roll accelerations.

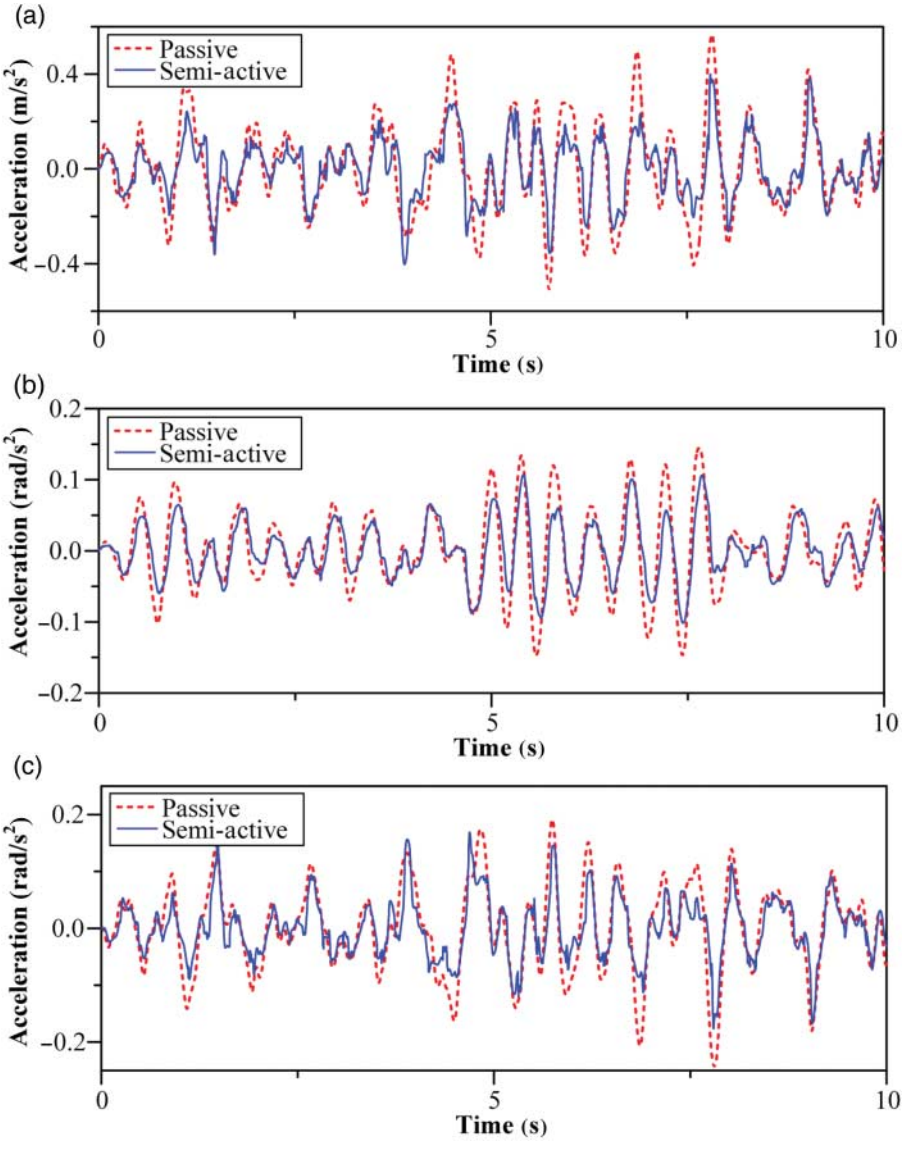

Figure 18. Time histories of the car body accelerations under the random track irregularities: (a) lateral accelerations, (b) yaw accelerations, and (c) roll accelerations.

Table 3. RMS and peak-to-peak values of the car body accelerations of the railway vehicles with different suspension systems (unit: lateral – m/s^2; yaw – rad/s^2; roll – rad/s^2).

	RMS values			Peak-to-peak values		
	Passive	Semi-active	Reduction (%)	Passive	Semi-active	Reduction (%)
Lateral $\ddot{y}_c$	0.1924	0.1307	32.1	1.0743	0.8024	25.3
Yaw $\ddot{\varphi}_c$	0.0571	0.0415	27.4	0.2915	0.2087	28.4
Roll $\ddot{\theta}_c$	0.0778	0.0537	30.9	0.4342	0.3452	20.5

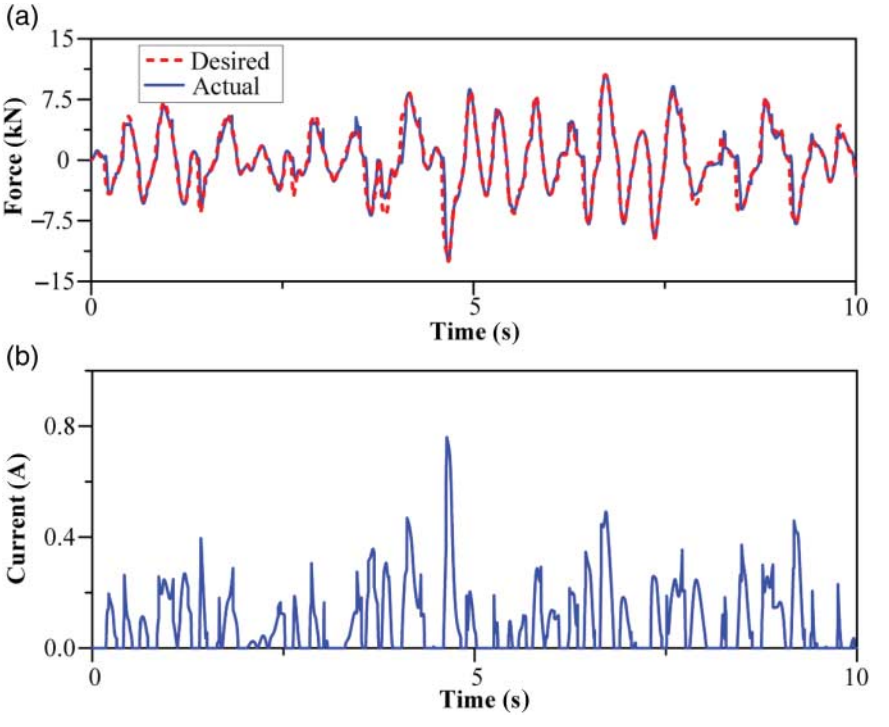

Figure 19. Time histories of the damping forces and the command current of the front MR dampers: (a) the desired and actual damping forces and (b) the command current.

From Figure 17, it can be found that the lateral and roll vibrations of the car body using semi-active suspension are lower than that of the car body using passive suspension, and the yaw vibrations using semi-active suspension are also lower than that using passive suspension except in the frequency range 0.7–1 Hz, where the yawing vibrations using semi-active suspension are a little bigger than that using passive suspension. The results indicate that the vibration attenuation ability of the semi-active suspension system is better than that of the passive suspension system.

Moreover, the semi-active suspension system shows better attenuation ability for the vibrations of the car body than the passive suspension system in the time histories (Figure 18). According to Tables 3, it can also be seen that the RMS and peak-to-peak values of the car body accelerations with the semi-active suspension system are lower than those with the passive suspension system, the reduction percentage of the RMS values is about 30%, and the reduction percentage of peak-to-peak values is near 25%. These also indicate that the ride quality of the railway vehicle with the semi-active suspension system is superior to that with the passive suspension systems.

Figures 19 and 20 show the time histories of the desired and actual damping forces of the front and rear MR dampers (u_1 and u_2) and the corresponding command currents, respectively. From Figures 19(a) and 20(a), it can be found that the actual damping force generated by the MR damper can well track the desired damping force, which further demonstrates that the ANFIS inverse model of the MR damper is effective in controlling the damping force. From Figures 19(b) and 20(b), it can be seen that the control currents change continuously in a low level, which indicate that the energy consumption of the semi-active suspension system is not too large.

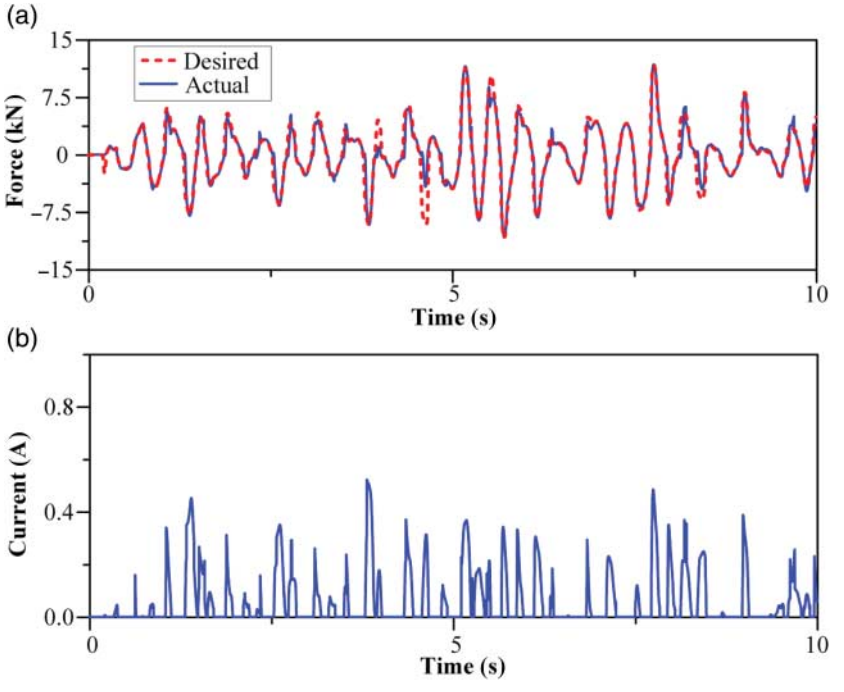

Figure 20. Time histories of the damping forces and the command current of the rear MR dampers: (a) the desired and actual damping forces and (b) the command current.

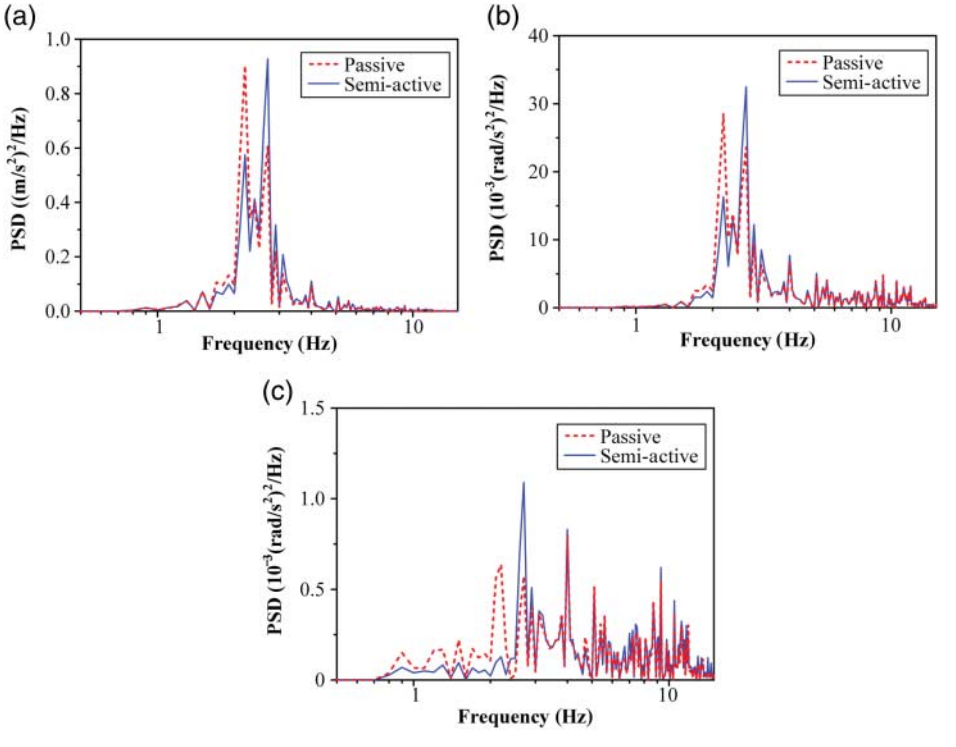

Figure 21. PSDs of the front bogie accelerations of the railway vehicles with different suspension systems under the random track irregularities: (a) lateral accelerations, (b) yaw accelerations, and (c) roll accelerations.

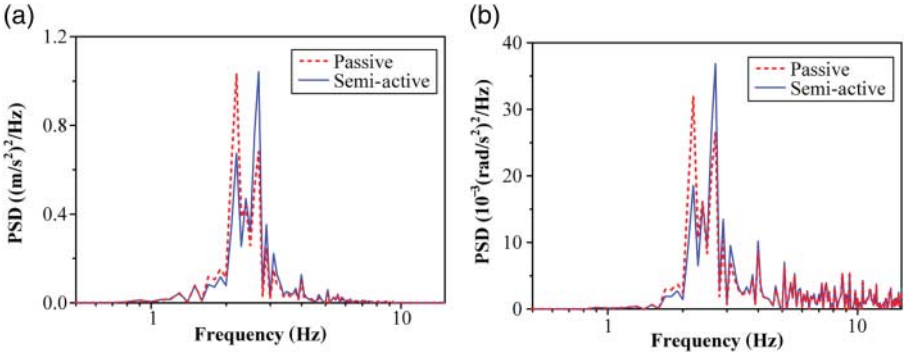

Figure 22. PSDs of the front bogie leading wheelset accelerations of the railway vehicles with different suspension systems under the random track irregularities: (a) lateral accelerations and (b) yaw accelerations.

Table 4. RMS values of the bogies and wheelsets accelerations of the railway vehicles with different suspension systems (unit: lateral – m/s^2; yaw – rad/s^2; roll – rad/s^2).

			RMS values		
			Passive	Semi-active	Reduction (%)
Bogies	Front	$\ddot{y}_{t1}$	1.6758	1.7160	−2.40
		$\ddot{\varphi}_{t1}$	0.4155	0.4136	0.47
		$\ddot{\theta}_{t1}$	0.1009	0.1106	−9.63
	Rear	$\ddot{y}_{t2}$	1.9142	1.9493	−1.83
		$\ddot{\varphi}_{t2}$	0.4568	0.4496	1.59
		$\ddot{\theta}_{t2}$	0.1045	0.1114	−6.64
Wheelsets	Lateral	$\ddot{y}_{w1}$	1.7625	1.8015	−2.21
		$\ddot{y}_{w2}$	1.5636	1.5906	−1.73
		$\ddot{y}_{w3}$	2.0121	2.0646	−2.61
		$\ddot{y}_{w4}$	1.7871	1.8157	−1.60
	Yaw	$\ddot{\varphi}_{w1}$	0.7507	0.7537	−0.40
		$\ddot{\varphi}_{w2}$	0.9660	0.9633	0.29
		$\ddot{\varphi}_{w3}$	0.7773	0.7751	0.29
		$\ddot{\varphi}_{w3}$	0.9925	0.9846	0.80

6.2. *Bogies and wheelsets accelerations*

The PSDs of the accelerations of the front bogie and the front bogie leading wheelset of the railway vehicles with the passive and semi-active suspensions under the random track irregularities are shown in Figures 21 and 22, respectively. The vibrations of the rear bogie are similar to that of the front bogie, and the vibrations of the other three wheelsets are similar to that of the front bogie leading wheelset, so they are not repeated here. The corresponding RMS values of the accelerations of the bogies and wheelsets are given in Table 4, respectively.

From Figures 21 and 22, it can be found that the vibrations of the bogie and wheelset in the first peak value with semi-active suspension system are lower than that with passive suspension, while situations are opposite in the second peak value. The first and second peaks represent the bogie lateral motion in the same direction and bogie lateral motion in the opposite direction, respectively. In the semi-active suspension system, the damping forces generated by the front and rear MR dampers are not always consistent not only on the magnitude but also on the phase, so the bogie lateral motions in the opposite direction are motivated more significantly, which causes the deterioration on the second peak compared with the passive suspension. In

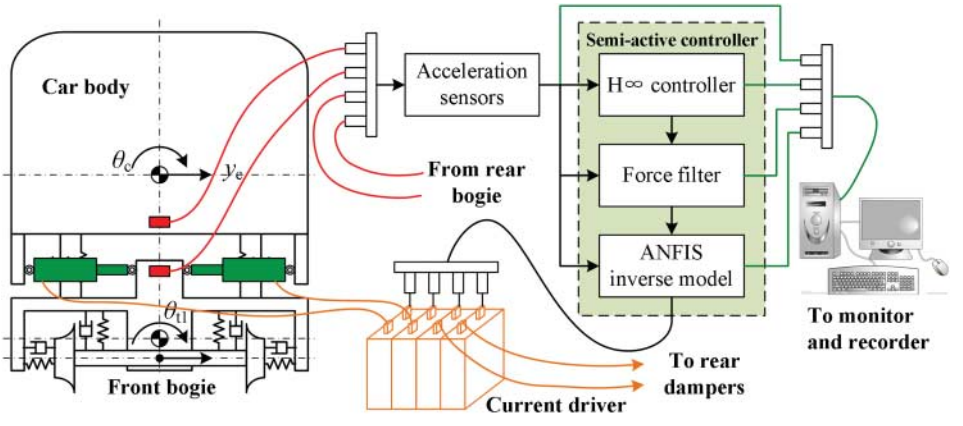

Figure 23. Schematic of the practical implementation for the MR damper-based semi-active controller.

general, the vibrations with the semi-active suspension system are almost similar to that with the passive suspension except for a little deterioration. According to Table 4, it can also be seen that the RMS values of the accelerations of the bogies and the wheelsets with the semi-active suspension system are nearly equal to those with the passive suspension system except for a little deterioration. In general, the semi-active suspension system does not suppress the vibrations of the bogies and wheelsets in comparison with passive suspension system, because the semi-active controller does not consider the dynamics of the bogies and wheelsets in order to simplify the design process and the number of the sensors.

Based on the above analysis, it can be concluded that the vibration of the high-speed train is reduced obviously by using MR dampers. These also indicate that MR dampers dissipate more energies compared with the ordinary dampers, namely they have higher energy dissipation efficiency.

7. Practical implementation

Figure 23 illustrates the schematic of the practical implementation for the proposed MR damper-based semi-active control system. The convenience in designing and less cost for practical use are the advantages of the proposed controller. In practical implementation, the whole control system works via five steps.

(1) First, the lateral accelerations of the connection points on the car body and the lateral accelerations of the bogies are measured by four acceleration sensors.
(2) Then, the H∞ controllers calculate the active control forces according to the measured outputs.
(3) Third, the force limiters generate the desired damping forces according to the active control forces.
(4) Fourth, the ANFIS inverse models of the MR dampers calculate the command currents of the MR dampers.
(5) Finally, the actual currents are generated by a current driver and inputted to the MR dampers to approximately track the desired damping forces. At the same time, the measured data and calculated data are also inputted into a computer to monitor the control system and record data.

8. Conclusions

This paper proposed an MR damper-based semi-active railway vehicle suspension system which is composed of a H∞ controller as the system controller and an ANFIS inverse model as the damper controller. After constructing the 17-DOF model of the railway vehicle, the forward and inverse dynamic models of the MR dampers and the H∞ controller made up of a yaw motion controller and a rolling pendulum motion controller, simulations are conducted to investigate the lateral, yaw, and roll accelerations of the car body, bogies, and wheelsets of the full-scale railway vehicle integrated with MR dampers under the random track irregularities. According to the simulations and analyses, the following conclusions can be drawn: (1) compared with the passive suspension system, the MR damper-based semi-active suspension system used for the railway vehicles can attenuate the lateral, yaw, and roll accelerations of the car body significantly (about 30%). (2) The vibrations of bogies and wheelsets with semi-active suspension system are almost similar to that with passive suspension except for a little deterioration. (3) The damper controller with the ANFIS inverse MR damper model is effective in tracking the desired damping force.

Acknowledgements

Financial supports from the National Natural Science Foundation of China (Grant No. 11125210) and the Fund of the Chinese Academy of Sciences for Key Topics in Innovation Engineering (Grant No. KJCX2-EW-L02) are gratefully acknowledged.

References

[1] W.H. Liao and D.H. Wang, *Semiactive vibration control of train suspension systems via magnetorheological dampers*, J. Intell. Mater. Syst. Struct. 14(3) (2003), pp. 161–172.
[2] M. Ahmadian and C.A. Pare, *A quarter-car experimental analysis of alternative semiactive control methods*, J. Intell. Mater. Syst. Struct. 11(8) (2000), pp. 604–612.
[3] M.M. ElMadany and Z.S. Abduljabbar, *Linear quadratic Gaussian control of a quarter-car suspension*, Veh. Syst. Dyn. 32(6) (1999), pp. 479–497.
[4] I.J. Fialho and G.J. Balas, *Design of nonlinear controllers for active vehicle suspensions using parameter-varying control synthesis*, Veh. Syst. Dyn. 33(5) (2000), pp. 351–370.
[5] I. Fialho and G.J. Balas, *Road adaptive active suspension design using linear parameter-varying gain-scheduling*, IEEE Trans. Control Syst. Technol. 10(1) (2002), pp. 43–54.
[6] H.P. Du, K.Y. Sze, and J. Lam, *Semi-active H-infinity control of vehicle suspension with magneto-rheological dampers*, J. Sound Vib. 283(3–5) (2005), pp. 981–996.
[7] S.B. Choi, H.S. Lee, and Y.P. Park, *H∞ control performance of a full-vehicle suspension featuring magnetorheological dampers*, Veh. Syst. Dyn. 38(5) (2002), pp. 341–360.
[8] A. Hac and I. Youn, *Optimal semi-active suspension with preview based on a quarter car model*, Trans. ASME, J. Vib. Acoust. 114(1) (1992), pp. 84–92.
[9] S.B. Choi, Y.T. Choi, and D.W. Park, *A sliding mode control of a full-car electrorheological suspension system via hardware-in-the-loop simulation*, Trans. ASME, J. Dyn. Syst. Meas. Control 122(1) (2000), pp. 114–121.
[10] M. Yu, C.R. Liao, W.M. Chen, and S.L. Huang, *Study on MR semi-active suspension system and its road testing*, J. Intell. Mater. Syst. Struct. 17(8–9) (2006), pp. 801–806.
[11] K.C. Schurter and P.N. Roschke, *Neuro-fuzzy control of structures using acceleration feedback*, Smart Mater. Struct. 10(4) (2001), pp. 770–779.
[12] M. Yu, X.M. Dong, S.B. Choi, and C.R. Liao, *Human simulated intelligent control of vehicle suspension system with MR dampers*, J. Sound Vib. 319(3–5) (2009), pp. 753–767.
[13] H.R. Oneill and G.D. Wale, *Semi-active suspension improves rail vehicle ride*, Comput. Control Eng. J. 5(4) (1994), pp. 183–188.
[14] V.S. Atray and P.N. Roschke, *Neuro-fuzzy control of railcar vibrations using semiactive dampers*, Comput. Aided Civil Infrastruct. Eng. 19(2) (2004), pp. 81–92.
[15] J.W. Yang, J. Li, and Y.P. Du, *Adaptive fuzzy control of lateral semi-active suspension for high-speed railway vehicle*, International Conference on Intelligent Computing, Kunming, 2006.
[16] P.E. Orukpe, X. Zheng, I.M. Jaimoukha, A.C. Zolotas, and R.M. Goodall, *Model predictive control based on mixed H-2/H-infinity control approach for active vibration control of railway vehicles*, Veh. Syst. Dyn. 46 (2008), pp. 151–160.

[17] D.H. Wang and W.H. Liao, *Semi-active suspension systems for railway vehicles using magnetorheological dampers. Part I: System integration and modelling*, Veh. Syst. Dyn. 47(11) (2009), pp. 1305–1325.
[18] D.H. Wang and W.H. Liao, *Semi-active suspension systems for railway vehicles using magnetorheological dampers. Part II: Simulation and analysis*, Veh. Syst. Dyn. 47(12) (2009), pp. 1439–1471.
[19] S.J. Dyke, B.F. Spencer, M.K. Sain, and J.D. Carlson, *Modeling and control of magnetorheological dampers for seismic response reduction*, Smart Mater. Struct. 5(5) (1996), pp. 565–575.
[20] O. Yoshida and S.J. Dyke, *Seismic control of a nonlinear benchmark building using smart dampers*, J. Eng. Mech. ASCE 130(4) (2004), pp. 386–392.
[21] Z.Q. Gu and S.O. Oyadiji, *Application of MR damper in structural control using ANFIS method*, Comput. Struct. 86(3–5) (2008), pp. 427–436.
[22] R. Stanway, J.L. Sproston, and N.G. Stevens, *Non-linear modelling of an electro-rheological vibration damper*, J. Electrost. 20(2) (1987), pp. 167–184.
[23] N.M. Wereley, L. Pang, and G.M. Kamath, *Idealized hysteresis modeling of electrorheological and magnetorheological dampers*, J. Intell. Mater. Syst. Struct. 9(8) (1998), pp. 642–649.
[24] W.H. Li, G.Z. Yao, G. Chen, S.H. Yeo, and F.F. Yap, *Testing and steady state modeling of a linear MR damper under sinusoidal loading*, Smart Mater. Struct. 9(1) (2000), pp. 95–102.
[25] B.F. Spencer, S.J. Dyke, M.K. Sain, and J.D. Carlson, *Phenomenological model for magnetorheological dampers*, J. Eng. Mech. ASCE 123(3) (1997), pp. 230–238.
[26] R. Jimnez and L. Alvarez, *Real time identification of structures with magnetorheological dampers*, 41st IEEE Conference on Decision and Control, Las Vegas, NV, 2002.
[27] Q. Zhou, S.R.K. Nielsen, and W.L. Qu, *Semi-active control of three-dimensional vibrations of an inclined sag cable with magnetorheological dampers*, J. Sound Vib. 296(1–2) (2006), pp. 1–22.
[28] N.M. Kwok, Q.P. Ha, T.H. Nguyen, J. Li, and B. Samali, *A novel hysteretic model for magnetorheological fluid dampers and parameter identification using particle swarm optimization*, Sens. Actuator A, Phys. 132(2) (2006), pp. 441–451.
[29] S.B. Choi, S.K. Lee, and Y.P. Park, *A hysteresis model for the field-dependent damping force of a magnetorheological damper*, J. Sound Vib. 245(2) (2001), pp. 375–383.
[30] C.C. Chang and L. Zhou, *Neural network emulation of inverse dynamics for a magnetorheological damper*, J. Struct. Eng. ASCE 128(2) (2002), pp. 231–239.
[31] K.C. Schurter and P.N. Roschke, *Fuzzy modeling of a magnetorheological damper using ANFIS*, 9th IEEE International Conference on Fuzzy Systems, San Antonio, TX, 2000.
[32] E.R. Wang, X.Q. Ma, S. Rakhela, and C.Y. Su, *Modelling the hysteretic characteristics of a magnetorheological fluid damper*, Proc. Inst. Mech. Eng. D, J. Automob. Eng. 217(D7) (2003), pp. 537–550.
[33] C. Sakai, H. Ohmori, and A. Sano, *Modeling of MR damper with hysteresis for adaptive vibration control*, 42nd IEEE Conference on Decision and Control, Maui, 2003.
[34] H.H. Tsang, R.K.L. Su, and A.M. Chandler, *Simplified inverse dynamics models for MR fluid dampers*, Eng. Struct. 28(3) (2006), pp. 327–341.
[35] D.H. Wang and W.H. Liao, *Modeling and control of magnetorheological fluid dampers using neural networks*, Smart Mater. Struct. 14(1) (2005), pp. 111–126.
[36] H. Wang and H.Y. Hu, *The fuzzy approximation of MR damper (in Chinese)*, J. Vib. Eng. 19(1) (2006), pp. 31–36.
[37] F.T. Wang, *Vehicle System Dynamics (in Chinese)*, China Railway Publishing House, Beijing, 1994.
[38] D.S. Garivaltis, V.K. Garg, and A.F. Dsouza, *Dynamic response of a six-axle locomotive to random track inputs*, Veh. Syst. Dyn. 9(3) (1980), pp. 117–147.
[39] M.H. Bhatti and V.K. Garg, *A review of railway vehicle performance and design criteria*, Int. J. Veh. Des. 5(1–2) (1984), pp. 232–254.
[40] H. Claus and W. Schiehlen, *Modeling and simulation of railway bogie structural vibrations*, Veh. Syst. Dyn. 29(1998), pp. 538–552.
[41] C. Guo and Z.W. Ming, *Numerical simulation of the stochastic process of railway track irregularities (in Chinese)*, J. Southwest Jiaotong Univ. 34(2) (2001), pp. 138–142.
[42] J.S.R. Jang, *ANFIS – adaptive-network-based fuzzy inference system*, IEEE Trans. Syst. Man Cybern. 23(3) (1993), pp. 665–685.
[43] H.Q. Zhang, *H∞optimal control of vehicle active suspension (in Chinese)*, Railw. Locomotive Car (2) (1996), pp. 43–48.
[44] J.W. Yang, *Study on semi-active control system for lateral vibration of high-speed vehicle (in Chinese)*, Ph.D. diss., China Academy of Railway Sciences, Beijing, 2006.

Appendix

Table A1. Parameter values and definitions of the 17-DOF railway vehicle model.

	Symbol	Value	Unit	Definition
Wheelset	m_w	1750	kg	Mass of wheelset
	J_{wz}	1400	kg m^2	Yaw moment of inertia of wheelset
	W	1.117×10^5	N	Load per wheelset
Bogie	m_t	3296	kg	Mass of bogie
	J_{tz}	2100	kg m^2	Yaw moment of inertia of bogie
	J_{tx}	1900	kg m^2	Roll moment of inertia of bogie
Car body	m_c	32,000	kg	Mass of car body
	J_{cz}	2.24×10^6	kg m^2	Yaw moment of inertia of car body
	J_{cx}	75,000	kg m^2	Roll moment of inertia of car body
Primary suspension	K_{1x}	2.9×10^7	N/m	Double of primary longitudinal stiffness
	K_{1y}	1.5×10^7	N/m	Double of primary lateral stiffness
	K_{1z}	1.33×10^6	N/m	Double of primary vertical stiffness
	C_{1x}	0	N s/m	Double of primary longitudinal damping
	C_{1y}	0	N s/m	Double of primary lateral damping
	C_{1z}	3.0×10^4	N s/m	Double of primary vertical damping
Secondary suspension	K_{2x}	3.4×10^5	N/m	Double of secondary longitudinal stiffness
	K_{2y}	3.5×10^5	N/m	Double of secondary lateral stiffness
	K_{2z}	6.8×10^5	N/m	Double of secondary vertical stiffness
	C_{2x}	5.0×10^5	N s/m	Double of secondary longitudinal damping
	C_{2y}	5.2×10^4	N s/m	Double of secondary lateral passive damping
	C_{2z}	1.6×10^5	N s/m	Double of secondary vertical damping
Size	h_1	0.763	m	Vertical distance from car body centre of gravity to secondary spring
	h_2	0.78	m	Vertical distance from car body centre of gravity to secondary lateral damper
	h_3	0.0245	m	Vertical distance from bogie frame centre of gravity to secondary spring
	h_4	−0.2085	m	Vertical distance from bogie frame centre of gravity to primary suspension
	h_5	0.2175	m	Vertical distance from bogie frame centre of gravity to secondary lateral damper
	l	9	m	Half of bogie centre pin spacing
	l_1	1.25	m	Half of wheelbase
	b	0.7465	m	Half of wheelset contact distance
	b_1	1	m	Half of primary suspension spacing (lateral)
	b_2	1	m	Half of secondary spring spacing (lateral)
	b_3	1	m	Half of secondary vertical damper spacing (lateral)
	r_0	0.4575	m	Wheel rolling radius
	V	300	km/h	Vehicle speed
Wheel rail parameters	f_{11}	1.12×10^7		Longitudinal creep coefficient
	f_{22}	9.98×10^6		Lateral creep coefficient
	λ_e	0.05		Effective wheel conicity
	σ	0.05		Wheelset roll coefficient
Track irregularities	Ω_c	0.438	rad/m	Truncated wavenumber
	Ω_r	0.8246	rad/m	Truncated wavenumber
	Ω_s	0.0206	rad/m	Truncated wavenumber
	A_a	10.80×10^{-7}		Scalar factor of lateral alignment
	A_v	6.125×10^{-7}		Scalar factor of cross-level